Iranian Journal of Chemistry and Chemical Engineering (IJCCE)

Silicon-acrylic core-shell structure containing phosphorous moiety: Synthesis, Research and Efficiency

Amir Hossein Moradifard[1], Ali Hassani Joshaghani[1,*], Hossein Mazaheri[1], Mahmoud Salimi[1], Khalil Faghihi[2]

[1]Department of Chemical Engineering, Arak Branch, Islamic Azad University, Arak, Iran

[2]Department of Chemistry, Faculty of Science, Arak University, Arak, Iran

[*]*Corresponding authors (E-mail: ali.hassani@iau.ac.ir, Fax: +98 863 413 4028)*

Abstract

In recent years, interest in improving the properties of polymers has become particularly important. Thermal stability is one of these properties that has been widely used in recent years due to its specific applications. One way to increase thermal stability is phosphorylation. Also, due to environmental concerns, a lot of attention is being paid to water-based latex. A butyl acrylate (BA)-silicone-acrylic copolymer was obtained by mini-emulsion polymerization. Nuclear magnetic resonance spectroscopy (NMR), scanning electron microscopy (SEM), dynamic light scattering (DLS), differential scanning calorimetry (DSC), and thermogravimetric analysis (TGA) analysis were used to thoroughly characterise the goods. DLS verified the presence of 80–100 nm-sized latex particles. DSC results revealed that the presence of silicone chains in the matrix, considering that silicone has a lower glass transition temperature than BA, reduces the glass transition temperature of the matrix and increases the flexibility of the chains. In addition, the presence of phosphorus in the copolymer chain increases the T_g. Formation of char for B5S5P3 due to the presence of phosphorus, causes a delay in the destruction of the sample and an increase in the temperature of the destruction of the matrix in TGA analysis. Also, the presence of silicon played a significant role in increasing thermal stability. Sample B5S5P3 with 30% phosphorus by mass showed first and second decomposition temperatures of 348 and 630 °C. In addition, in the flame analysis, the B5S5P3 sample showed the best combustion performance among other samples.

Keywords: Phosphorylation; Silicon, Mini-emulsion; Copolymer; Degradation; Glass transition temperature.

Introduction

In recent years, polymer coating has gained great importance and acceptance due to its suitable chemical and physical properties, wide applications, availability and reasonable price [1-9]. Meanwhile, water-based coatings have gained a special place due to environmental issues and ease of use. Emulsion polymerization is an appropriate technique for water-based coatings since it is more environmentally friendly than solvent technology and more energy-efficient than hot melt technology. [10-19]. As one of the widely used substrates in water-based coatings, acrylic polymers have anti-UV properties (due to the lack of double bonds), oxidation resistance, colorlessness, and relatively suitable temperature tolerance. The flexibility of coating is an important factor for their use in different fields. The use of silicone in the polymer chains of adhesives not only increases the flexibility of the polymer chains but also increases the heat resistance of the coatings [20-23]. These characteristics enable the application of unique coatings to various industrial materials, sensors, electronics structural materials, and aerospace materials. In many special applications, it is necessary to increase the resistance of the coating to heat and flame. This operation is performed in various ways, such as the addition of inorganic nanoparticles and phosphorylation. Phosphorylation of polymer matrices is one of the traditional methods in this field. In addition to improving the thermal properties of coatings, they also improve conductivity, corrosion protection and lubricity. [24-29].

The numerous qualities and uses of acrylate coating synthesis have garnered interest. Park et al. created a silicone-acrylic paint-based resin that is extremely weather resistant for use in construction materials [30]. They employed 3-methacryloxypropyltrimethoxysilane (MPTS) as the acrylic monomer-reactive silicone monomer and n-butyl acrylate, methyl methacrylate, and n-butyl methacrylate as the acrylic monomers. All samples had a glass transition temperature of 30 °C and contained 10, 20, and 30 weight percent of MFTS [30]. They verified that while viscosity and average molecular weight rose, MPTS's thermal stability improved as silicone content rose. Satisfactory results were seen in gloss retention, yellowness difference, color difference, and brightness difference in both the outdoor exposure test and the accelerated test. In another work, Kan et al. prepared a copolymer of styrene–butyl acrylate–silicone via Semi-continuous emulsion method [31]. The results showed that for samples containing less than 25% by weight of silicon, the conversion percentage reached 86%. This may be due to self-condensation and polycondensation of silicon. The silicon content is less than 20%, so the surface adhesion and flexibility are very good. When this amount exceeds 25%, the amount of adhesion decreases due to a decrease in polarity [31]. However, the impact properties increased as the amount of silicon increased. The enhancement of the thermal properties of these polymers along with their environmental properties has increased in recent years. Illy et al. performed another

method to phosphorylate polysaccharide. This matrix is widely used in the field of tissue engineering scaffolds, where causal binding results in fouling [25].

In this study, a BA-silicone-acrylic copolymer was obtained by mini-emulsion polymerization. Phosphorus is added to the polymer matrix to improve thermal properties. The polymer matrix was identified using NMR analysis. Thermal properties were tested after adding phosphorus to the polymer chain using TGA analysis.

Experimental

Materials

Sodium dodecyl sulfate (SDS, 99%>purity) and tetraisoproxide titanate (TPT, 98%>purity) were purchased from Sigma-Aldrich (Multinational company). All of the solvents and monomers with 99% purity including methyl ethyl ketone (MEK), and potassium persulfate (KPS), sodium hydrogen carbonate ($NaHCO_3$), Triton X-100, butyl acrylate (BA), hexadecane (HD), hydroxyl-terminated silicone (Z-6018), Hydroxyethyl methacrylate (HEMA) and H_3PO_4 (ortho-phosphoric acid, 85%>purity) were supplied by Merck Chemical Co. (Multinational company). All recipes employed deionized (DI) water, and all chemicals were used without additional purification.

Characterization

^{1}H-NMR provided support for the synthesised compounds' chemical structures and functional groups. Using tetramethylsilane (TMS) as the internal reference, a 400 MHz instrument (BRUKER, Germany) was used to record the ^{1}H-NMR spectra in DMSO-d6. Using DLS, the particle size and particle size distribution (PSD) of each sample were ascertained. After each sampling, the samples were diluted 100 times using an aqueous solution of surfactants that had concentrations comparable to the polymerization recipe using a Brookhaven-nanobrook omni (US) at a laser angle of 90º. Tescan Vega II (Czech Republic) equipment was used to SEM images. Using an EMITECH K450x sputter-coater (England), one drop of the diluted latex was deposited on a sample holder, dried under vacuum at 25ºC, and then sputter coated with gold powder. A NETZSCH-Maia 200-F3 (Germany) calorimeter was used to perform DSC analyses between -150 and 120ºC (scanning rate of 10 ºC/min) while nitrogen gas was flowing through it. Using the METTLER TOLEDO (TGA1 model, Switzerland) thermogravimetric analysis (TGA) at a heating rate of 10°C/min (25−800 °C) in N_2 environment, the thermal stability of the produced copolymers was evaluated.

Preparation of silicon acrylate monomer

A four-necked round-bottom flask held 105 g of Z-6018 (0.38 mol), 0.5 g of TPT (0.0017 mol), 0.5 g of cupric chloride ($CuCl_2$, 0.0037 mol), and 70 cc of toluene. The HEMA (0.38 mol) weighed 50 g was then added dropwise and maintained at 80 °C. The HEMA was finally poured dropwise, and while stirring, the temperature was increased to 120°C. After removing unreacted HEMA from the reaction mixture using distilled water, it was dried on anhydrous Na_2SO_4. Based on HEMA, the yield was 90% [31] (Figure 1).

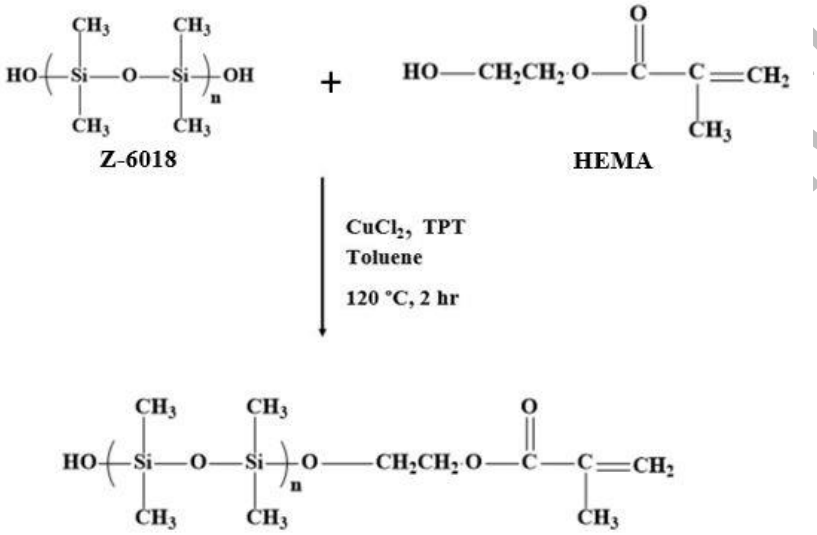

Figure 1. Synthesis of silicone acrylate monomer.

Preparation of butyl acrylate-silicon copolymer

An aqueous solution of 0.24 g SDS (as anionic surfactant, 0.0008 mol), 0.12 g Triton X-100 (as nonionic surfactant, 0.00019 mol), 0.12 g sodium bicarbonate (as buffer, 0.0014 mol), 0.12 g potassium persulfate (as initiator, 0.00043 mol) and 48 ml of deionized water are mixed. A mixture of BA, acrylate silicone and HD (0.12 g, 0.00045 mol) was then added to the solution and the whole mixture was probe sonicated for 15 min (68 W, 20 kHz). The temperature was brought to 75 ºC and stirred mechanically (450 rpm) for 5 h in a continuous stream of nitrogen gas. No coagulum was observed at the end of the polymerization and the final monomer conversion was greater than 95% gravimetrically.

Phosphorylation of BA-silicon copolymers

There are several methods for phosphorylate aromatic and aliphatic compounds that have OH groups. One of these methods is to esterify compounds using H_3PO_3 and H_3PO_4. Phosphorus can be covalently bonded to compounds containing OH, and this bonding through OH leads to the formation of the structure shown in Figure 2.

Figure 2. Covalently connections of OH to phosphorus [21].

In addition, since these derivatives directly bond with phosphorus and contain mobile hydrogen groups in tautomeric equilibrium, phosphorus-containing compounds can be obtained. Distilled water was used to dilute phosphoric acid to a 60% by weight concentration. After that, the mixture was agitated for an hour at 95 °C in a water bath while urea was added in a 1:8 ratio (urea/H_3PO_4). Butyl compound was added to the acid solution after an hour, and it was then left in a water bath at 95° C for two hours without being stirred. After being taken out of the water bath, the phosphorylated compounds were vacuum-dried for eight hours at 60 °C (Figure 3).

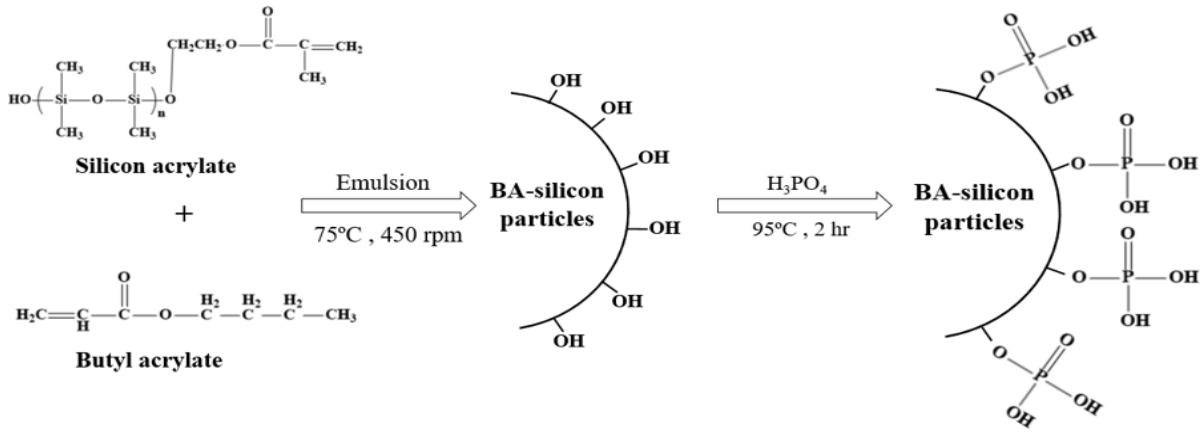

Figure 3. Schematic diagram of the steps for the synthesis of BA-silicon chains containing phosphorus groups.

Table 1 shows the composition of polymer matric in the polymerization that is used in the syntheses of silicon acrylate copolymers and phosphorized copolymers.

Table 1. Composition of polymer matric in the polymerization.

Sample[a]	BA (w%)	Silicon (w%)	Phosphorous[*] (w%)
B9S1	90	10	0
B7S3	70	30	0
B5S5	50	50	0
B9S1P1	90	10	10
B7S3P2	70	30	20
B5S5P3	50	50	30

a Amounts of $NaHCO_3$, KPS, HD and Triton X-100 were all 0.12 g and SDS was 0.24 g in each recipe.

*The percentage of phosphorus relative to the total amount of Si+BA

Results and Discussion

^{1}H-NMR spectrum of sample B5S5 was recorded to confirm the synthesis and chemical structure (Figure 4). A characteristic singlet peak of the methyl group protons of the silicon fragments was found in the range of 0 to 1 ppm. The Appearance of a singlet peak at 5 ppm for hydroxyl protons, along with a triplet at 4-4.5 ppm, indicates the incorporation of a silicone moiety into the polymer chain. As shown in Figure 4, the hydrogens related to e, g and k have triplet peaks, and hydrogens of i, j and h in the range of 4-5 ppm also have triplet peaks. By using TPT, self-condensation of the silicone intermediate is prevented and the intended condensation between silanol-OH and acrylic-OH is encouraged [32-34].

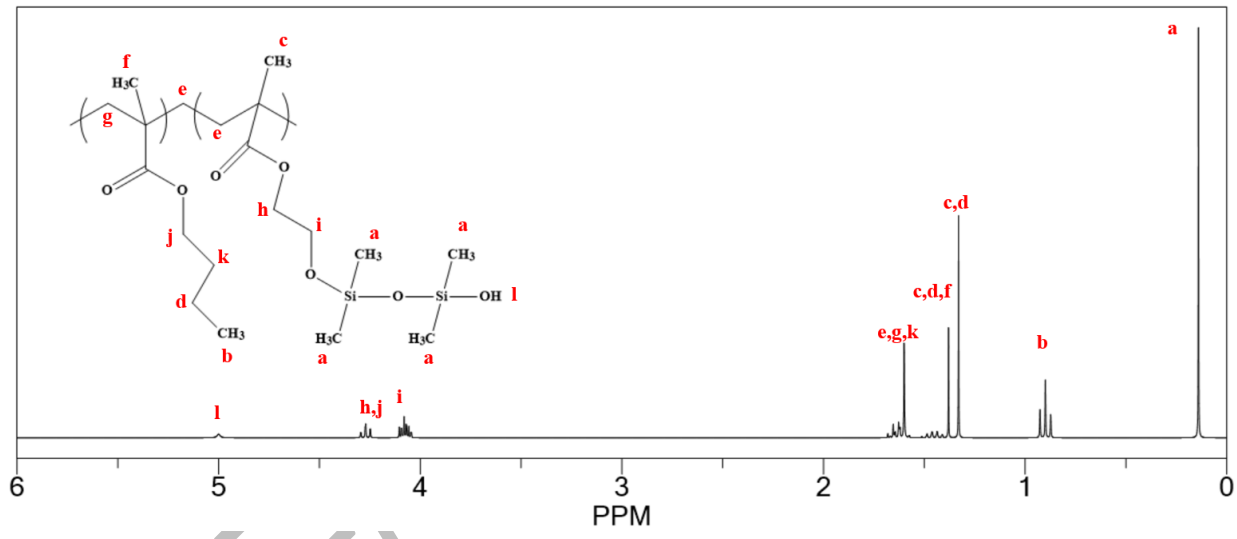

Figure 4. ^{1}H-NMR spectrum (400 MHz) of BA-HEMA-Silicon copolymer in DMSO-d6 at 298K.

SEM and DLS analysis conducted on B9S1, B7S3, and B5S5 latexes have been depicted in Figure 5 and Figure 6. As you can see in the images, the latex particles are spherical (in Figure 5a, 5b particles are stuck together in some areas) and the particle size is less than 100 nm. Particle size was unaffected substantially by varying the copolymer weight ratio. The SEM micrographs and PSD demonstrate the restricted size distribution of the latex particles. Consequently, it was discovered that the silicone mass fraction and butyl acrylate mass fraction had no effect on the latex particle size. [35, 36].

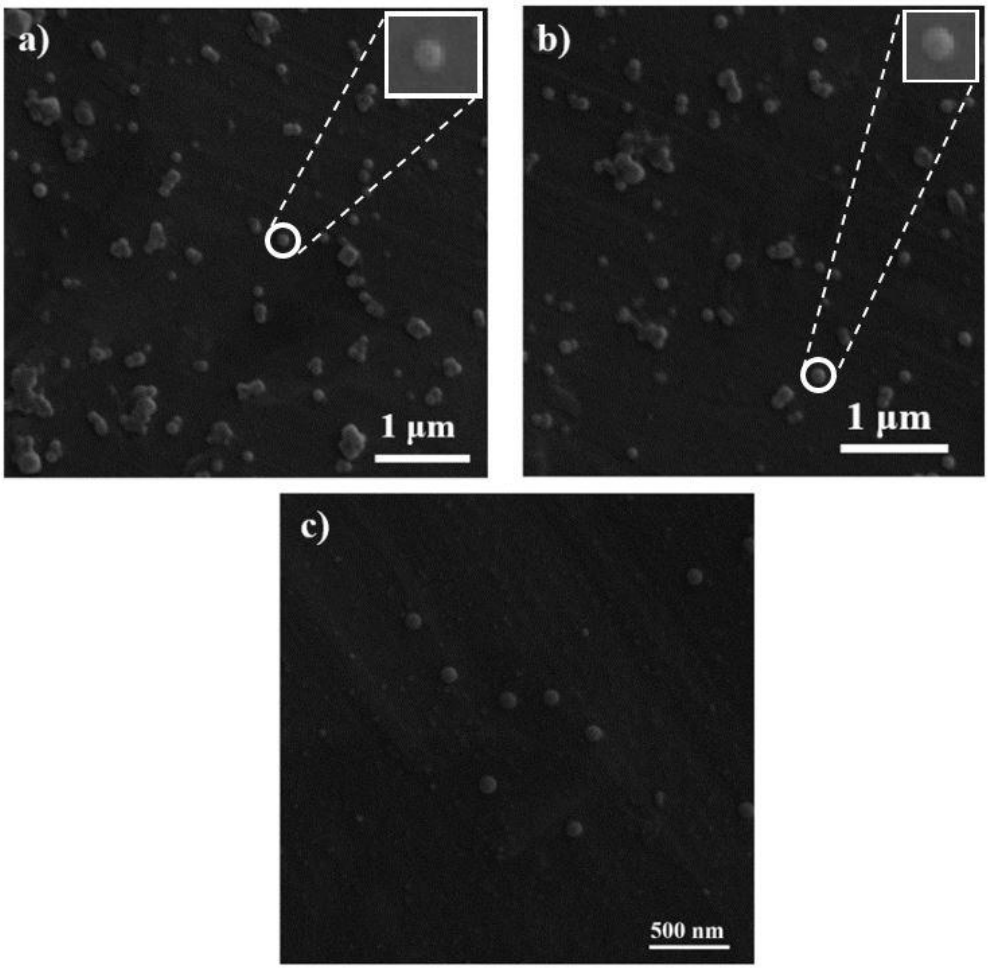

Figure 5. SEM images of a) B9S1, b) B7S3 and c) B5S5 latex.

As shown in Figure 6, the DLS curves for the B9S1, B7S3 and B5S5 latexes are displayed. The curves are unimodal and sharp, indicating adequate polymerization and lack of secondary nucleation during polymerization. The size of the particles obtained from polymerization is in the range of 85-90 nm. The presence of silicon in the chain has increased the size of the particles to an insignificant amount, but the PSD indicates proper polymerization and the formation of spherical particles with the highest degree of monodispersity in polymerization.

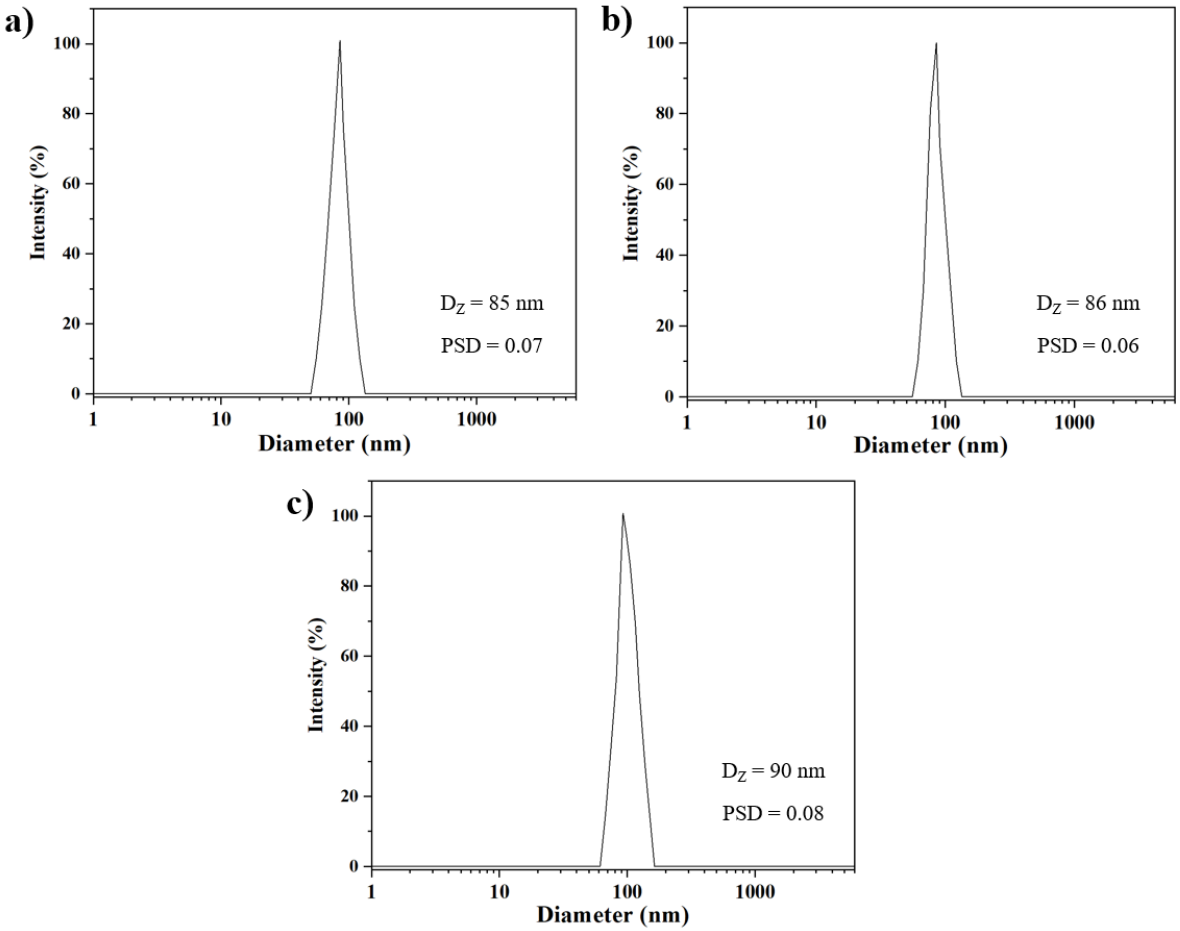

Figure 6. DLS curves of a) B9S1, b) B7S3 and c) B5S5 latexes.

DSC analysis was used to confirm the correctness of the copolymerization. The experimental glass transition temperature ($(T_g)_{exp}$) is compared with the theoretical glass transition temperature ($(T_g)_{theo}$) that was computed via the Fox equation [37] (Eq. 1).

$$\frac{1}{T_{g(t)}} = \frac{w_1}{T_{g(1)}} + \frac{w_2}{T_{g(2)}} \quad \text{(Eq. 1)}$$

$T_{g(1)}$ is the glass transition temperature of the first matrix, $T_{g(2)}$ is the glass transition temperature of the second matrix, and $T_{g(t)}$ is the overall glass transition temperature in Eq. 1. w_1 and w_2 are the weight fractions of the first and second matrices, respectively.

The incomplete transformation of the polymerization reaction and the volatility of the monomers are the causes of the various variances between the $(Tg)_{theo}$ and $(Tg)_{exp}$. Figure 7 displays the DSC thermograms of samples B9S1, B7S3, and B5S5. The findings demonstrated that lowering the copolymer's glass transition temperature by adding more silicone to the mass fraction increased the chain's flexibility. This reduction in glass transition temperature is also a very important factor in bonding applications. However, in samples containing phosphorus, due to the presence of phosphorus

and OH crosslinking, the intermolecular distance increases for this reason and the mobility of polymer chains decreases, resulting in an increase in the glass transition temperature.

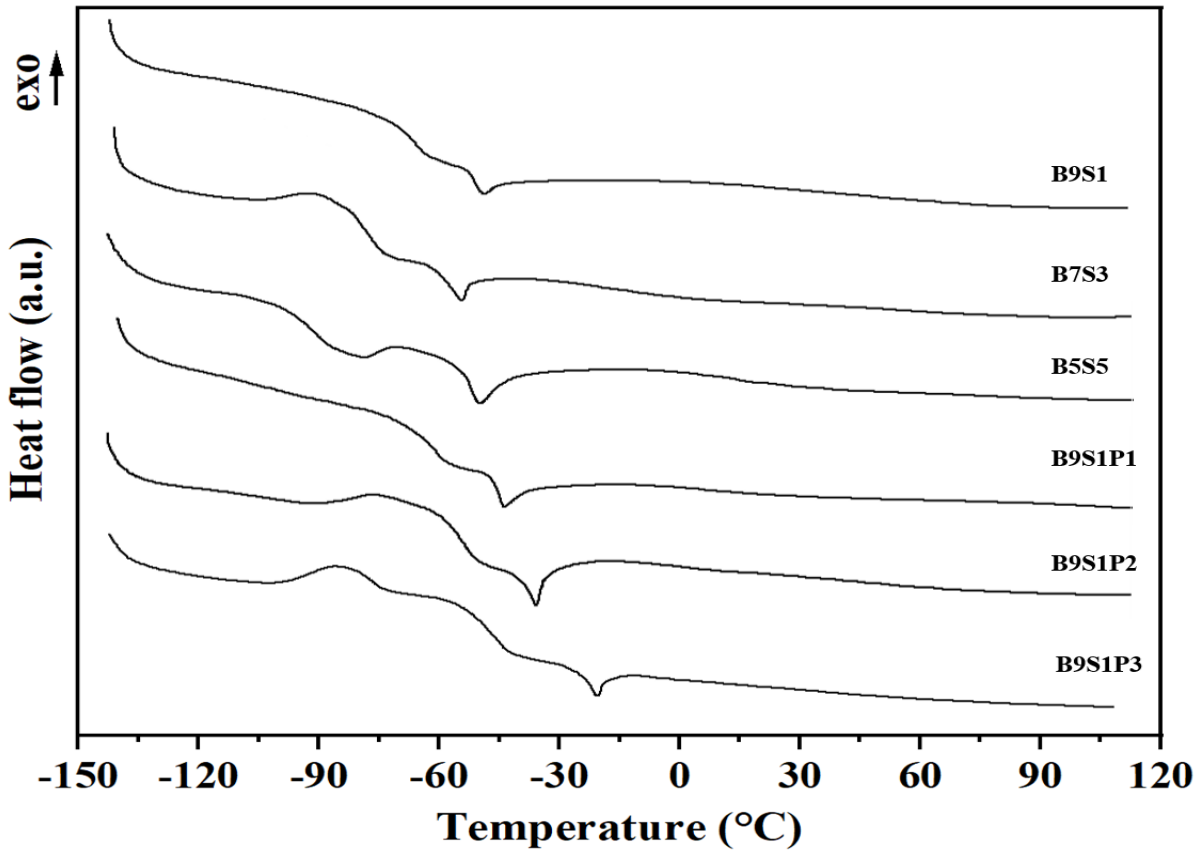

Figure 7. DSC curves of polymer matrices with and without phosphorus.

The glass transition temperature for each sample is displayed in Table 2. As it is clear in the diagram, the crystallization temperature of silicon and its melting temperature are -73 and -40 °C, respectively, which due to the presence of phosphorus and the created thermal stability caused the shift of melting and crystallization temperature [38-40].

Table 2. Comparison between $(T_g)_{theo}$ and $(T_g)_{exp}$ of samples.

Sample	$(T_g)_{theo}$ (°C)	$(T_g)_{exp}$(°C)	Si content (wt.%)	P content (wt.%)
B9S1	-61	-70	10	0
B7S3	-74	-83	30	0
B5S5	-87	-95	50	0
B9S1P1	-61	-64	10	10
B7S3P2	-74	-60	30	20
B5S5P3	-87	-49	50	30

The use of flame retardants in polymer materials and composites alters the polymer's weight loss characteristics in the TGA analysis (Figure 8). In fact, the phosphorus groups used as flame retardants in polymers decompose at low temperatures to form heat-resistant carbons, allowing the polymer matrix to decompose at high temperatures. In the first analysis, the thermal stability of composite materials containing phosphorus includes two stages. In the first step, phosphorus is decomposed at low temperatures and converted to charcoal. In the second step, the polymer matrix decomposes at a temperature of 300-400 °C. Silicon migrates to the surface of the material to form a protective layer against oxidative pyrolysis due to its low surface energy and high antioxidant stability at high temperatures.

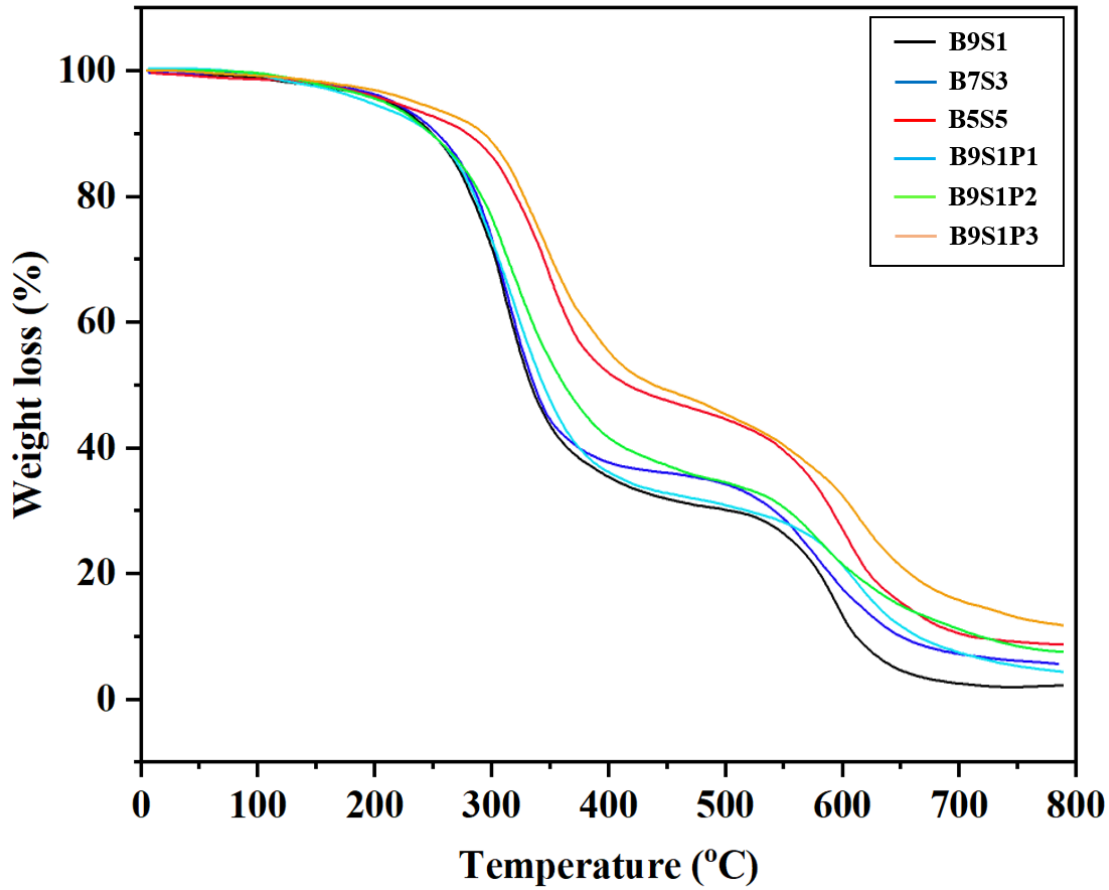

Figure 8. TGA curves of samples with and without phosphorus moiety.

Table 3 shows the temperature of the decomposition of the first stage (FSD) and the decomposition of the second stage (SSD).

Table 3. Comparison between T_{FSD} and T_{SSD} of samples.

Sample	T_{FSD}	T_{SSD}	Si content (wt.%)	P content (wt.%)	Char ratio at 800°C
B9S1	307	575	10	0	5
B7S3	309	574	30	0	7
B5S5	340	600	50	0	10
B9S1P1	311	585	10	10	7
B7S3P2	320	583	30	20	8
B5S5P3	348	630	50	30	12

As shown in Figure 8, sample B9S1 containing 10% silicone has a two-step mass loss, the first step at 250-350 °C is related to the decomposition of butyl acrylate. Due to its higher thermal stability and migration to the surface, during decomposition, silicon is transported at a higher temperature and decomposes in the temperature range of 400 °C. In B7S3 and B5S5, the proportion of the body increased as the amount of silicon in the polymer chain increased. The temperature range of each stage is shown in Table 1. Also, due to the increase in silicon, the carbon residual content increased relatively from 7% to 10%. After adding phosphorus to the polymer chain, the weight loss process includes changes. In B9S1P1, which contains 10% by weight of phosphorus, the observed weight loss was transferred to higher temperatures in two stages. The reason for this is that phosphorus begins to burn at temperatures lower than the decomposition temperature of the first stage and forms charcoal. The formation of charcoal causes heat to be transferred to the polymer matrix with a delay and the process of decomposition of the polymer matrix occurs at higher temperatures. In B7S3P3, which contains 30% by weight of phosphorus, it was observed that the amount of delay in decomposition is much higher and occurs at higher temperatures. Additionally, more carbon residues were observed at the end of the analysis, which correlated with higher phosphorus content. It can be concluded that two factors simultaneously play a role in the thermal stability of the matrix. The first element is silicon, which positively increases the thermal stability of the matrix, and the second element is phosphorus, which makes the polymer matrix resistant to heat due to the formation of charcoal. The synergistic effect of these two elements created favorable thermal properties of the butyl acrylate matrix and the final product [33, 40-42].

Figure 9 shows images of the original BA-silicon matrix and BA-silicon-phosphorus flame retardant composites after burning according to ASTM E136-65. Testing was conducted at a temperature of 650ºC. In Figure 9, it can be seen the degree of burning of the film surface for the phosphorus-free sample. In the phosphorus-free sample, the sample surface was severely deformed because it could not retain heat. The addition of phosphorus to the polymer matrix greatly increased the ability of the matrix to withstand heat. The reason is that when phosphorus is exposed to heat, it burns to form

char, and the formation of this char retards the combustion of the matrix. Sample B9S1P1 with 10% phosphorus showed less burning than sample B9S1. Increasing the percentage of phosphorus in sample B5S5P3 to 30% makes this sample the most stable.

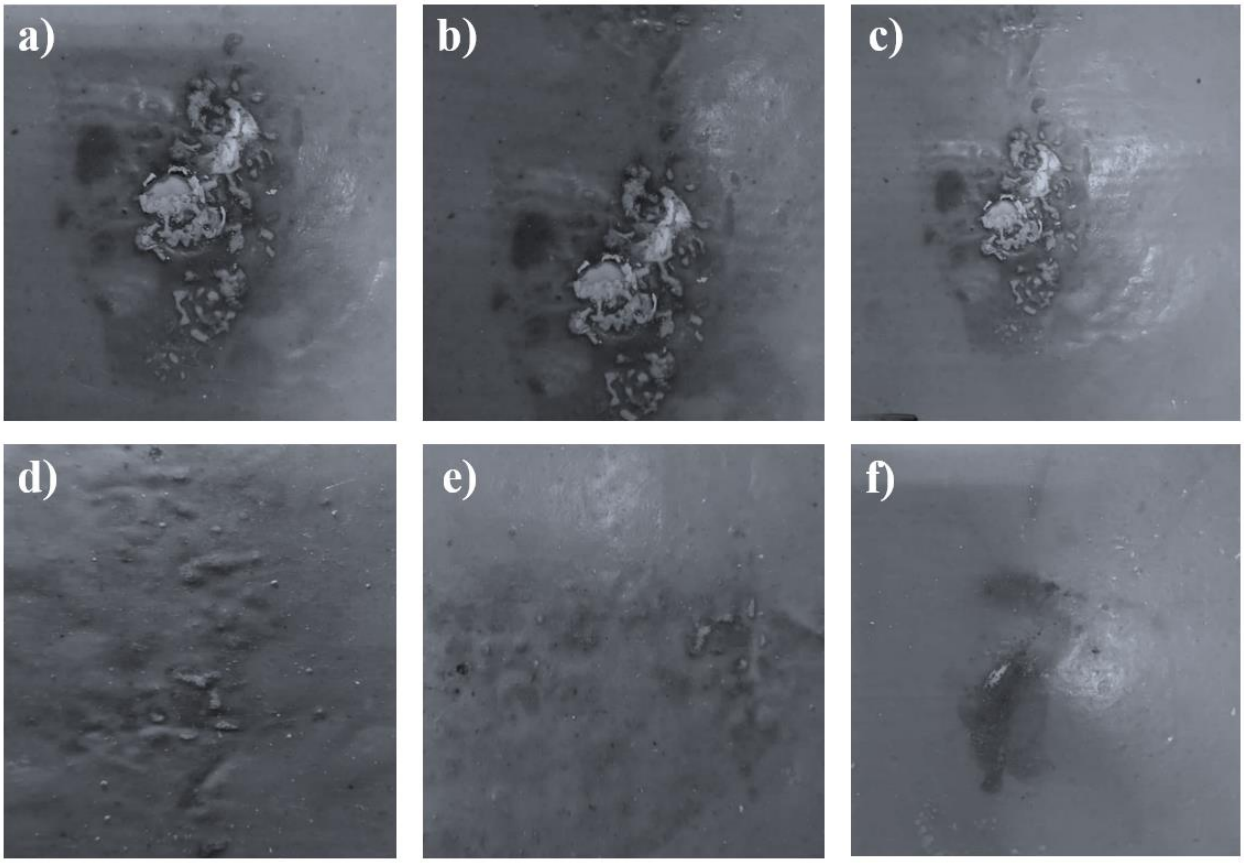

Figure 9. Photographs of final residues of a) B9S1, b) B7S3, c) B5S5, d) B9S1P1, e) B7S3P2 and f) B5S5P3 after combustion.

Conclusion

A BA-silicone copolymer containing phosphorus was synthesized. The stability obtained by adding phosphorus was confirmed by TGA and burning analysis. DLS and SEM analyses showed that the size of the final polymerized particles was between 80 and 100 nm and that the addition of phosphorus did not change the size of the final particles. TGA analysis results show that the addition of phosphorus to the polymer chains creates a heat barrier and transfers the weight loss associated with the polymer matrix to higher temperatures. The decomposition temperatures of sample B5S5P3 with the highest phosphorus content are 348 °C and 630 °C, respectively. In addition, the results showed that increasing the mass fraction of silicon relative to phosphorus-free samples increased the stability of the polymer matrix. In this regard, we can conclude that the influence of silicon and phosphorus on the increase in thermal stability is unavoidable and these two factors coincide with each other. The fire resistance of

sample B5S5P3 was very evident. The surface of the film did not burn at a temperature of 650 °C, and this result shows that the phosphorus groups play a good role and increase the thermal stability of the matrix.

References

[1]. Khotbehsara, M. M., Manalo, A., Aravinthan, T., Turner, J., Ferdous, W., & Hota, G., Effects of ultraviolet solar radiation on the properties of particulate-filled epoxy based polymer coating, *Polymer Degradation and Stability*, 181, 109352 (2020).

[2]. Ilango, N. K., Gujar, P., Nagesh, A. K., Alex, A., & Ghosh, P., Interfacial adhesion mechanism between organic polymer coating and hydrating cement paste, *Cement and Concrete Composites*, 115, 103856 (2021).

[3]. Liu, F., Lin, Z., Jin, Q., Wu, Q., Yang, C., Chen, H. J., ... & Xie, X., Protection of nanostructures-integrated microneedle biosensor using dissolvable polymer coating, *ACS applied materials & interfaces*, 11(5), 4809-4819 (2019).

[4]. Somnet, K., Thimoonnee, S., Karuwan, C., Kamsong, W., Tuantranont, A., & Amatatongchai, M., Ready-to-use paraquat sensor using a graphene-screen printed electrode modified with a molecularly imprinted polymer coating on a platinum core, *Analyst*, 146(20), 6270-6280 (2021).

[5] Othman, N. H., Ismail, M. C., Mustapha, M., Sallih, N., Kee, K. E., & Jaal, R. A., Graphene-based polymer nanocomposites as barrier coatings for corrosion protection, *Progress in Organic Coatings*, *135*, 82-99 (2019).

[6] Barroso, G., Li, Q., Bordia, R. K., & Motz, G., Polymeric and ceramic silicon-based coatings–a review, *Journal of materials chemistry A*, *7*(5), 1936-1963 (2019).

[7] Seifi, M. H., Sharifzadeh, M., Ghorbani, M., & Omidkhah, M. R., Study on synthesis of doped polyaniline with alumina and its anticorrosion properties as an additive in paint coating, *Iranian Journal of Chemistry and Chemical Engineering* (2023).

[8] Ullah, A., Mushtaq, A., Ahmed, Q. R., Ali, Z. U., Rashid, A., Afshan, S., ... & Zamzam, Z. Experimental Analysis of Polymer-Coated Aggregate in Comparison to Ordinary Road Material. *Iran. J. Chem. Chem. Eng. Research Article Vol*, *41*(8) (2022).

[9] Rahayu, D. U. C., Nurandini, I. A., Veristya, V. S., Yunarti, R. T., & Nizardo, N. M. Study of the Effect of Poly (ethylene glycol) on the Nifedipine Microencapsulation and Release. Iran. J. Chem. Chem. Eng. Research Article Vol, 41(8) (2022).

[10] Shahbazi, N., Rajaei, A., Tabatabaei, M., Mohsenifar, A., & Bodaghi, H. Impact of chitosan-capric acid nanogels incorporating thyme essential oil on stability of pomegranate seed oil-in-water Pickering emulsion. Iranian Journal of Chemistry and Chemical Engineering, 40(6), 1737-1748 (2021).

[11] Ullah, W., Gul, H., Ullah, R., Gul, S., Ali Shah, A. U. H., & Bilal, S. Corrosion Inhibition Properties of Sulfonated Polyaniline-Poly (Vinyl Alcohol) Composite on Mild Steel. Iranian Journal of Chemistry and Chemical Engineering, 41(4), 1313-1321(2022).

[12] Dhar, A., Bhattacharjee, M., Barman, J., Talukdar, H., & Haloi, D. J., Synthesis and characterization of starch-g-poly (methyl methacrylate-co-styrene) copolymer prepared via emulsion polymerization. *Iranian Journal of Chemistry and Chemical Engineering*, *42*(4), 1314-1319 (2023).

[13] Ahmed Khan, I., Hussain, H., & Yasin, T., Fabrication and characterization of amidoxime-grafted silica composite particles via emulsion graft polymerization. *Iranian Journal of Chemistry and Chemical Engineering*, 39(5), 111-120 (2020).

[14]. Kozakiewicz, J., Trzaskowska, J., Domanowski, W., Kieplin, A., Ofat-Kawalec, I., Przybylski, J., ... & Sylwestrzak, K., Studies on Synthesis and Characterization of Aqueous Hybrid Silicone-Acrylic and Acrylic-Silicone Dispersions and Coatings, Part I. *Coatings*, 9(1), 25 (2019).

[15]. Cardoso, A. P., de Sá, S. C., Beraldo, C. H., Hidalgo, G. E., & Ferreira, C. A., Intumescent coatings using epoxy, alkyd, acrylic, silicone, and silicone–epoxy hybrid resins for steel fire protection, *Journal of Coatings Technology and Research*, 17(6), 1471-1488 (2020).

[16]. Kim, S. K., & Park, H. J., Preparation and Physical Properties of Acrylic Silicone Resin Coatings Using Warer Dispersed Acrylic Resin, *In Proceedings of the Korean Institute of Building Construction Conference* (pp. 162-163). (2021).

[17]. Kim, S. K., & Park, H. J., Preparation and Physical Properties of Acrylic Resin Coatings Containing Tertiary Amine and Epoxysilane Curing Agent, *In Proceedings of the Korean Institute of Building Construction Conference* (pp. 164-165) (2021).

[18] Le, T. T., Nguyen, T. V., Nguyen, T. A., Nguyen, T. T. H., Thai, H., Dinh, D. A., & Nguyen, T. M., Thermal, mechanical and antibacterial properties of water-based acrylic Polymer/SiO2–Ag nanocomposite coating, *Materials Chemistry and Physics*, 232, 362-366 (2019).

[19] Sardari, A., Alvani, A. A. S., & Ghaffarian, S. R., Castor oil-derived water-based polyurethane coatings: Structure manipulation for property enhancement, *Progress in Organic Coatings*, 133, 198-205 (2019).

[20]. Zelepukin, I. V., Mashkovich, E. A., Lipey, N. A., Popov, A. A., Shipunova, V. O., Griaznova, O. Y., ... & Zvyagin, A. V., Direct photoacoustic measurement of silicon nanoparticle degradation promoted by a polymer coating, *Chemical Engineering Journal*, 430, 132860 (2022).

[21]. Li, S., Lin, X., Liu, Y., Li, R., Ren, X., & Huang, T. S., Phosphorus-nitrogen-silicon-based assembly multilayer coating for the preparation of flame retardant and antimicrobial cotton fabric, *Cellulose*, 26(6), 4213-4223 (2019).

[22]. Zhang, J., Liang, Z., Liu, J., Wan, Y., Tao, X., Zhang, H., & Wang, M., Preparation and performance analysis of palygorskite reinforced silicone-acrylic emulsion-based intumescent coating, *Progress in Organic Coatings*, 166, 106801 (2022).

[23]. Izmitli, A., Ngunjiri, J., Lan, T., Pacholski, M. L., Smith, R., Langille, M., ... & Manna, J., Impact of silicone additives on slip/mar performance and surface characteristics of waterborne acrylic coatings, *Progress in Organic Coatings*, 131, 145-151 (2019).

[24] Wu, C. S., Liu, Y. L., Chiu, Y. C., & Chiu, Y. S., Thermal stability of epoxy resins containing flame retardant components: an evaluation with thermogravimetric analysis, *Polymer degradation and stability*, 78(1), 41-48 (2002).

[25] Illy, N., Fache, M., Menard, R., Negrell, C., Caillol, S., & David, G., Phosphorylation of bio-based compounds: the state of the art, *Polymer Chemistry*, 6(35), 6257-6291 (2015).

[26] Hsiue, G. H., Liu, Y. L., & Tsiao, J., Phosphorus-containing epoxy resins for flame retardancy V: Synergistic effect of phosphorus–silicon on flame retardancy, *Journal of Applied Polymer Science*, 78(1), 1-7 (2000).

[27] Li, J., Wang, H., & Li, S., A novel phosphorus– silicon containing epoxy resin with enhanced thermal stability, flame retardancy and mechanical properties, *Polymer Degradation and Stability*, 164, 36-45 (2019).

[28] Ouarga, A., Noukrati, H., Iraola-Arregui, I., Elaissari, A., & Barroug, A., Development of anti-corrosion coating based on phosphorylated ethyl cellulose microcapsules, *Progress in Organic Coatings*, 148, 105885 (2020).

[29] Chen, Z., Yu, Y., Zhang, Q., Chen, Z., Chen, T., & Jiang, J., Preparation of phosphorylated chitosan-coated carbon microspheres as flame retardant and its application in unsaturated polyester resin, *Polymers for Advanced Technologies*, 30(8), 1933-1942 (2019).

[30] Park, H. S., Yang, I. M., Wu, J. P., Kim, M. S., Hahm, H. S., Kim, S. K., & Rhee, H. W., Synthesis of silicone–acrylic resins and their applications to superweatherable coatings, *Journal of Applied Polymer Science*, 81(7), 1614-1623 (2001).

[31] Kan, C. Y., Liu, D. S., Kong, X. Z., & Zhu, X. L., Study on the preparation and properties of styrene–butyl acrylate–silicone copolymer lattices, *Journal of applied polymer science*, 82(13), 3194-3200 (2001).

[32] Kanai, T., Mahato, T. K., & Kumar, D., Synthesis and characterization of novel silicone acrylate–soya alkyd resin as binder for long life exterior coatings, *Progress in Organic Coatings*, 58(4), 259-264 (2007).

[33] Xu, L., Xu, L., Dai, W. S., & Tsuboi, T., Preparation and characterization of a novel fluoro-silicone acrylate copolymer by semi-continuous emulsion polymerization, *Journal of Fluorine Chemistry*, *153*, 68-73 (2013).

[34] Ghorbani, R. E., Zohuri, G. H., & Gholami, M., Novel synthesis method and characterization of poly (vinyl acetate-butyl acrylate) latex particles: effect of silanol-terminated poly (dimethylsiloxane) surfactant on the seeded emulsion copolymerization, *Journal of Surfactants and Detergents*, *20*, 891-904 (2017).

[35] Wang, Y., & Fang, S., Preparation and characterization of cationic silicone-acrylic latex surface sizing agent. *Progress in Organic Coatings*, *88*, 144-149 (2015).

[36] Carter, M. C., Miller, D. S., Schork, F. J., Ratani, T. S., Lan, T., Woodworth, R. P. & Mecca, J. M., Nonionic Surfactants Promote the Incorporation of Silicone–Acrylic Hybrid Monomers in Emulsion Polymerization. *ACS Applied Polymer Materials*, *4*(7), 4829-4838 (2022).

[37] Brostow, W.; Chiu, R.; Kalogeras, I. M.; Vassilikou-Dova, A. Prediction of Glass Transition Temperatures: Binary Blends and Copolymers, *Mater. Lett*., 62, 3152–3155 (2008).

[38] Lin, M., Chu, F., Guyot, A., Putaux, J. L., & Bourgeat-Lami, E., Silicone–polyacrylate composite latex particles. Particles formation and film properties. *Polymer*, *46*(4), 1331-1337 (2005).

[39] Liu, J., Chen, L. Q., Li, W., & Zhang, L. M., Modified Polyacrylate-Based Latexes Containing Silicone. *Journal of Macromolecular Science, Part A*, *41*(8), 913-925 (2004).

[40] Chen, L., Shao, T., & Gong, Y., Synthesis and characterization of fluoro-silicone polyacrylate latex emulsified with novel green surfactants. *Progress in Rubber, Plastics and Recycling Technology*, *35*(2), 102-114 (2019).

[41] Wei, S. Q., Bai, Y. P., & Shao, L., A novel approach to graft acrylates onto commercial silicones for release film fabrications by two-step emulsion synthesis. *European Polymer Journal*, *44*(8), 2728-2736 (2008).

[42] Li, X., Bian, F., Hu, J., Li, S., Gui, X., & Lin, S., One-step synthesis of novel multifunctional silicone acrylate prepolymers for use in UV-curable coatings, *Progress in Organic Coatings*, *163*, 106601 (2022).